Article

The Legacy of Mercury Contamination from a Past Leather Manufacturer and Health Risk Assessment in an Urban Area (Pisa Municipality, Italy)

Lisa Ghezzi * [iD], Simone Arrighi, Roberto Giannecchini [iD], Monica Bini [iD], Marta Valerio and Riccardo Petrini [iD]

Department of Earth Science, University of Pisa, Via S. Maria 53, 56126 Pisa, Italy; simone.arrighi@unipi.it (S.A.); roberto.giannecchini@unipi.it (R.G.); monica.bini@unipi.it (M.B.); martavalerio94@gmail.com (M.V.); riccardo.petrini@unipi.it (R.P.)
* Correspondence: lisa.ghezzi@unipi.it

Abstract: An abandoned open green space in the urban setting of the Municipality of Pisa (Tuscany, Italy) has been designed for renewal to foster the development of recreational activities and improve the lives of the surrounding communities. However, the geochemical site characterization revealed Pb, Cu, Zn and Hg concentrations in the soil exceeding the thresholds imposed by Italian regulations for residential use. Pb, Cu and Zn contents likely reflect the effects of urban vehicle traffic, while Hg contamination represents the legacy of a past artisanal tannery that used Hg(II)-chloride in leather processing in the mid-1900s. Mercury is widely distributed in the area, with the highest concentration in the uppermost soil layer, and reaching about 170 mg/kg in the common dandelion rhizosphere. Chemical extractions and thermal desorption experiments have indicated that most Hg is in the elemental free and matrix-bound fraction, with a possible minor amount (less than 4 wt%) of HgS and negligible methylated forms (0.1 wt%). The data suggest that soil processes could reduce Hg^{2+} to volatile Hg^0. Mercury in groundwater, hosted in a shallow aquitard in the area, was below 0.2 µg/L. However, the presence of chloride in groundwater might result in the formation of Hg stable aqueous complexes, increasing Hg release from solids. Future water quality monitoring is hence recommended. The risk assessment highlighted that mercury in soil carries a risk of non-cancerous effects, in particular for children, posing the basis for management planning.

Keywords: mercury contamination; mercury speciation; urban area; risk analysis

1. Introduction

Mercury is highly toxic for humans, ecosystems, and wildlife (e.g., [1–4]) and has been included among the ten chemicals of major health concern by the World Health Organization [5]. In particular, organic mercury is a potent neurotoxin [6] which accumulates in the biota and becomes biomagnified in the food chain [7,8], representing an important route for human exposure. Inorganic mercury is generally found in the environment in different oxidation states as elemental Hg^0 that can be converted to vapor at ambient temperature due to its low latent heat of evaporation: mercuric ion Hg^{2+} and mercurous ion Hg_2^{2+}. The latter is metastable and rarely investigated in natural settings [9], since it is expected to be rapidly disproportionate to elemental mercury and Hg^{2+} complexes. The organometallic compounds of Hg_2^{2+} are also scarce, whereas mercuric ions in water and soil may be readily converted to organic methylmercury (MeHg, CH_3Hg^+) and re-methylated to form dimethylmercury (DMeHg, CH_3HgCH_3) across a great diversity of bacterial species [10]. In particular, methylation under reducing conditions primarily occurs through the role of sulfate-reducing bacteria [11–13]. Indeed, methylation is a complex process [14–20], and methylation rates depend on a large number of physico-chemical and biological factors, including the total amount of Hg^{2+} [21] and the occurrence of specific molecules (e.g., [22]). Demethylation may occur through abiotic and biotic processes [23], and the extent of MeHg

in the ecosystem is the result of both methylation and demethylation processes. Hg^{2+} in the water–soil system may form a variety of complexes and matrix-bound compounds, and it is mostly sorbed by natural organic matter [24–27], Mn-Fe oxy-hydroxides [28,29], and clays. Hg^{2+} can be reduced by Fe^{2+}-bearing minerals through surface reactions and by humic substances [30–35] yielding the formation of gaseous Hg^0. Mercury vapor may also be sorbed by soil, and transformation to mercuric form may occur. Under favorable conditions, Hg^{2+} reacts with sulfur sources leading to the formation of the sparingly soluble cinnabar (α-HgS) and metacinnabar (β-HgS). This process inhibits Hg^{2+} methylation and immobilizes mercury in soils and sediments, even though some studies report that HgS in nanoparticles may be a source of MeHg [36]. Since mercury is not degraded by the ecosystem, many cases of present-day Hg contamination are a legacy from the past, adding further complexity in the assessment of contaminated sites. Major anthropogenic sources for mercury include chloralkali plants [37], cement production [38], iron and steel production [39], coal burning [40], mining [41–43], and oil refinement [44]. Mercury compounds have been widely used in the past as biocides and preservatives in a variety of applications, before their use became highly restricted or forbidden. In particular, mercury chlorophenol ($C_6H_5ClHgO_3$) and mercuric chloride ($HgCl_2$) were extensively applied in cereal and leather tanneries, leaving behind a large risk to the soil/aquifer system. Indeed, traditional tanning processes produced putrefied solid wastes and wastewaters with high concentrations of inorganic salts, heavy metals, and organics, although cleaner approaches to leather processing have been more recently developed [45]. In Italy, tanneries are generally characterized as small–medium size enterprises, often concentrated within municipalities, as in the tanning district of the Tuscany region [46].

Quantifying the total Hg content in soil is not sufficient for assessing the risk of an exposed population; it is necessary to determine the bioaccessible, soluble, and soil Hg vapor fractions. In the literature, several procedures have been proposed to quantify mercury fractionation and speciation [47], including thermal desorption and chemical sequential extraction procedures, even if inconsistent results have been obtained in some cases [48]. It is worth noting that consensual protocols for mercury speciation and certified materials for some Hg species are still lacking.

In the present study, the mercury environmental issues related to the legacy of a small bovine leather tanning manufacturer in an abandoned area within the Municipality of Pisa (Tuscany, Italy) have been investigated. In this context, the aim of this work was to evaluate the impact of Hg contamination in an urban area by determining concentration patterns, as well as the geochemical factors that contribute to mercury's fate. Specifically, the major objectives were: (i) to determine the degree of Hg distribution in soil and groundwater; (ii) to investigate the Hg speciation in soil using thermal desorption and sequential extraction methods; and (iii) to assess the health risk of exposure to mercury within a requalification project for the urban area.

2. Site Location and Geomorphological Outlines

The study area was located in the center of the Municipality of Pisa (Tuscany, Italy) (Figure 1), approximately 0.5 km south of the Leaning Tower and Cathedral Place (the so-called "Square of Miracles"), a UNESCO World Heritage Site. The city of Pisa is located in an alluvial plain, a flat low-lying area with a mean elevation of about 2.5 m a.s.l., bounded by the Ligurian Sea to the west, the Serchio River to the north, the Mt. Pisani to the east, and crossed by the Arno River (Figure 1a). An abrupt change in elevation is recorded in the proximity of the study area; indeed, the area east of the medieval city walls has an elevation of about 5 m a.s.l., whereas the area to the west is located at about 2.5 m a.s.l. (Figure 1b). The reason for this change in elevation is not totally clear [49].
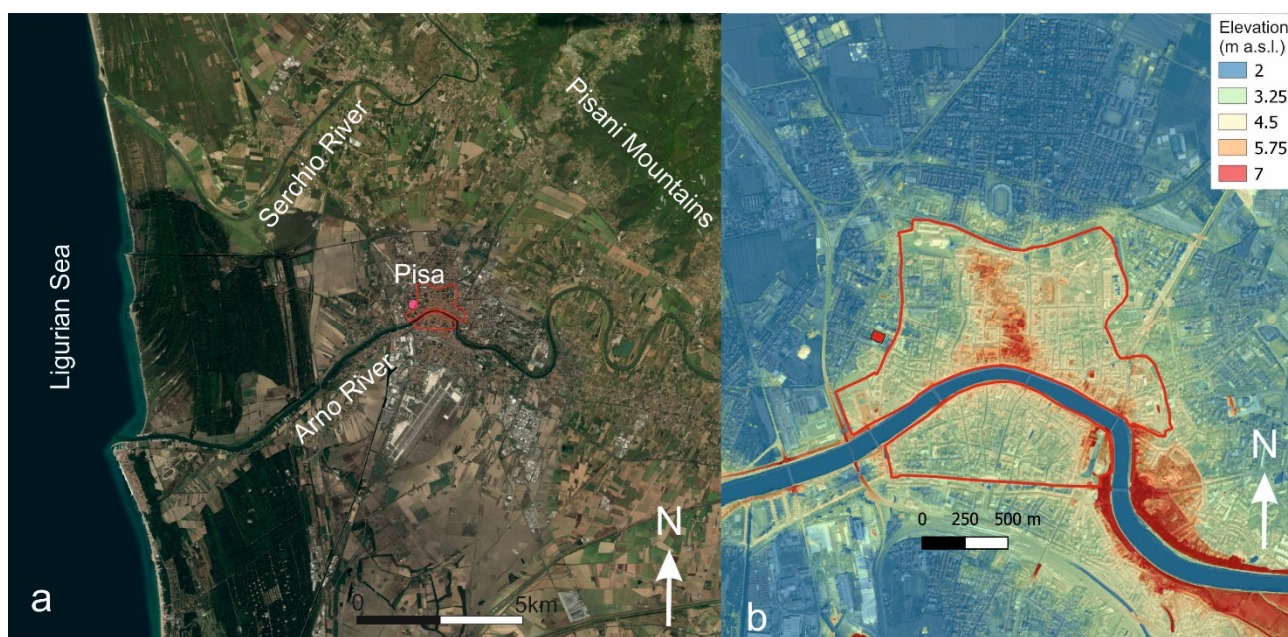
Figure 1. (**a**) The Pisa plain area (base map: Bing images) with indicated study site (red dot). (**b**) The study area (red square) in the context of the topographic features of the Pisa urban area. The red line represents the medieval city walls (base map DTM obtained from LiDAR data).

Since protohistoric times, this area has been characterized by a dense hydrographic network related to the combined fluvial activity of the Arno and Serchio rivers [50]. These highly sinuous and low-gradient rivers have frequently changed their course over time, as documented by several geomorphological studies. In particular, a north–south palaeochannel located between 9 and 13 m below ground level was identified nearby the study area [51]. During the last glacial–interglacial transition (MIS 2–MIS 1), the Arno River played a dominant role in the sedimentary and geomorphological evolution of the Pisa plain, forming a prominent incised valley, 40–45 m deep and 5–8 km^2 wide [52]. This palaeovalley was developed in response to the last phase of sea-level fall (culminating in the Last Glacial Maximum) and was progressively filled with estuarine and paludal deposits during the Late Glacial–Early Holocene transgression (about 13,000–8000 cal yr BP). The valley-fill succession is overlain by a laterally extensive, 3–15 m thick lagoonal unit composed of soft grey clays, accumulated approximately between 8000 and 5000 cal yr BP at the time of maximum marine ingression and during the early phases of sea-level highstand. Upwards is a 10–15 m thick deltaic alluvial sedimentary wedge originating from approximately 5000 yr BP. Eneolithic swamp clays, 1–3 m thick, form the lower portion of the late highstand fluvial succession and exhibit upward transition to poorly drained and then well-drained floodplain fine-grained deposits of protohistoric and historic age, respectively. Isolated to locally amalgamated fluvial-channel sand bodies, crevasse/levee sands and sand–silt alternations occur at different stratigraphic profiles. This progradational trend was temporarily interrupted by widespread backswamp development in Pisa's city center at the transition from the Iron age to the early Etruscan age. Stratigraphic profiles and hydrogeological context revealed the occurrence of a silty horizon, about 8 m thick, of alluvial origin with interbedded lenses of sandy deposits forming an aquitard. This succession is bordered below by a continuous sandy level representing the main semi-confined aquifer.

The study site consisted of an abandoned green space (about 1500 m^2) adjacent to the medieval defensive walls surrounding the city of Pisa, and was being included in an urban renewal project to become an important public playground and recreational site for inhabitants and tourists. A reconstructed history of the activities on the site revealed that a slaughterhouse operating from the middle of the 19th century to the 1960s was

located about 0.1 km south of the study area. Bovine hides were transferred from the slaughterhouse to a small artisanal tannery, located in the area under study, to be processed into leather. The tannery plants were built without any treatment facilities and environment management systems; as a result, hazardous metals including mercury (in the form of $HgCl_2$ powder) were discharged directly into the soil. After the tanning activity ceased, the derelict infrastructures were removed to improve the urban landscape without performing any appropriate environmental reclamation work.

3. Materials and Method

3.1. Sampling

In order to assess the current state of mercury pollution, soil, groundwater and plant environmental media were considered. An illustration of the spatial distribution of sampling stations is given in Figure 2. Two boreholes (PZ1 and PZ2) were drilled in July 2019 by non-destructive techniques, reaching the depth of 9 m below ground level. The extruded cores were collected and carefully stored in plastic core boxes. The cores were examined and cut into sections using a stainless-steel cutter; the outer layer in contact with the core tube was removed to eliminate possible contaminations. Two samples were taken from each drilling at depths between 0.1 m and 1.0 m (samples PZ1-A and PZ2-A), and between 1.2 m and 1.6 m (samples PZ1-B and PZ2-B) in accordance with Italian regulations for risk analysis. Each sample was mixed thoroughly to give a 1 kg composite. An additional borehole (PZ3) was drilled, reaching the depth of 3.0 m below ground level in order to investigate the soil and subsoil layer sequence in more detail. In PZ3 samples were collected from the core at nine different depths from ground level: PZ3-1 (0.31–0.34 m); PZ3-2 (0.54–0.57 m); PZ3-3 (0.82–0.85 m); PZ3-4 (1.11–1.14 m); PZ-5 (1.31–1.34 m); PZ3-6 (1.80–1.84 m); PZ3-7 (2.22–2.24 m); PZ3-8 (2.54–2.56 m); PZ3-9 (2.79–2.81 m). Soil was also collected throughout a trench (2 m wide, 1 m deep) excavated by a ditching machine. A 1 kg composite sample was collected along the full length of the exposed face of the trench, obtaining a composite sample (sample T1-A, 0.1–0.5 m), and one sample was collected from the bottom (sample T1-B, 1 m). During sampling, larger (>20 mm) fragments were removed in the field. Spatially distributed rhizosphere soils surrounding naturally growing dandelion (Taraxacum officinale) plant roots were collected in November 2018 (samples R1 to R12, Figure 2). In order to study the Hg migration from soil to roots and leaves, and to evaluate the exposure to gaseous Hg, the roots and leaves of dandelion were collected in correspondence with rhizosphere stations. One plant of dandelion taken from outside the contaminated area was transferred in a vase in order to prevent Hg uptake from soil and left in the site nearby station R4 from April 14 to May 27, 2019.

All soil samples were air-dried for 24 h to reduce Hg^0 losses [53]. Soils from boreholes were sieved to 2 mm in order to compare contaminant concentration against guideline values.

Dandelion roots were cleaned to carefully remove soil particles; roots and leaves were washed with Milli-Q water, dried at ambient temperature and ground in a mortar.

Boreholes PZ1 and PZ2 were equipped with PVC piezometers with a screen interval between 3 and 6 m below ground level in order to collect groundwater from the aquitard, as the water body most prone to contamination. Groundwater was collected from the PZ1 and PZ2 piezometers in two surveys in July 2019 (groundwater low-stage condition, samples PZ1_W1 and PZ2_W1) and January 2020 (groundwater high-stage condition, samples PZ1_W2 and PZ2_W2) using a low-flow (0.5 L/min) plastic 12 V pump, after purging. Water samples were filtered in the field through 0.45 μm nylon filters and refrigerated in pre-cleaned polyethylene bottles. Ultrapure nitric acid was used as a preservative for major cation and trace element analysis.

Figure 2. Sampling stations (PZ: boreholes/piezometers; T: trench; R: rhizosphere).

3.2. Analytical Procedures

Soil samples from boreholes PZ1 and PZ2 and trench T1 were digested by using a Milestone Ethos Easy microwave platform (US EPA Method 3051A). The concentration of a set of elements was determined by ICP-MS using a Perkin Elmer NexION 300X. The analytical uncertainty was evaluated by the analysis of the soil reference material NIST SRM 2711a. In general, the accuracy was better than 10%. Precision values, as relative standard deviation, were better than 5% for Li, Be, Mn, Ni, Ag, Sn, Cd, Tl, Pb, Fe and As, and within 10% for Co, Cu, Zn, Sr, Sb, Ba, Th, U, V, and Cr. Hexavalent Cr was measured following the US EPA Method 3060A. Total organic carbon (TOC) was determined according to EN 15936:2012. Additionally, soil pH was measured [54].

The total mercury content in borehole (PZ1, PZ2 and PZ3), trench (T1) and rhizosphere soil (samples R1 to R12), water (PZ1_W1, PZ1_W2 and PZ2_W1, PZ2_W2) and plants (samples R1 to R12) was determined by a Milestone DMA-80 (US EPA Method 7473). Repeated analysis of NIST 2711a (Montana soil), ERM-CC018 (contaminated sandy soil), MESS-3 (marine sediment) were used as reference materials. RSD and accuracy were less than 10%.

In order to quantify the Hg species in PZ1-A and PZ2-A soils, mercury speciation was investigated by sequential chemical extraction according to [55]; the average value for Hg recovery was $86 \pm 5\%$. Methyl-Hg analyses were performed using the extraction scheme proposed by [56] and approved by the Tuscany Region Environmental Protection Agency. The elemental mercury fraction in soil was estimated by thermal desorption techniques: continuous heating experiments from ambient temperature to 250 °C were performed by weighting about 50 mg of soil samples into a 250 mL borosilicate glass flask in a heating furnace. Temperature was digitally controlled to ± 1 °C; the applied heating rate ranged from 8 to 35 °C/min. Hg-release curves during heating were recorded by measuring the vapor emission by online Lumex RA-915M, using air flow as a carrier.

On-site measurements were conducted to determine the Hg gas release of the soil using a probe assembly inserted at a depth of 50 cm into the ground nearby the PZ1 station. Mercury soil gas was extracted by connecting a syringe to the probe and collected (after purging) through Carulite sorbent traps and analysed by Milestone DMA-80.

Water physico-chemical parameters (temperature, pH, electrical conductivity (EC), redox potential (Eh), and dissolved oxygen (DO)) from PZ1_W1, PZ1_W2 and PZ2_W1, PZ2_W2 were measured in the field. Alkalinity (expressed as HCO_3^-) was determined by acidimetric titration. Major ions were determined by ion chromatography using Thermo

Fisher ICS 900. RSD was less than 5%. Trace elements were determined by ICP-MS using a PerkinElmer NexIon 300X. The water reference solutions NIST SRM 1640a and 1643f were analysed. Deviations from the certified values (20 replicates) were less than 5%, except for As, Ba, Cr, Cu, Fe, Li, V (5–10%), and Zn (10–12%). Precision was better than 10% RSD.

3.3. Risk Assessment

In the present study, the mercury risk assessment was performed using a site-specific approach [57,58] and the Risk-net software (version 3.1.1, September 2019, available at http://www.reconnet.net/Software.htm (accessed on 21 February 2022)). The exposure routes considered were shallow soil ingestion, dermal contact, particulate inhalation, and outdoor vapour. Human receptors were identified for both adults and children.

The Hazard Quozient (HQ) for non-carcinogenic chronic effects in humans was calculated for each exposure pathway. In case of direct ingestion and dermal contact, HQ (i.e., $HQ_{ingestion}$ and HQ_{dermal}) was calculated by dividing the chronic daily intake (CDI, mg/kg/day) by the corresponding reference dose (RfD, mg/kg/day) [59–61], defined as the maximum daily exposure to a toxic agent that would not produce any appreciable deleterious effects on human health:

$$HQ = \frac{CDI}{RfD}$$

where CDI represents the exposure to a toxic agent, averaged over a long period of time, through ingestion (CDI_{ing}) or dermal contact (CDI_{derm}):

$$CDI_{ing} = C_{POE} * \frac{R_{ing} * EF * ED}{BW * AT} * 10^{-6}$$

$$CDI_{derm} = C_{POE} * \frac{SA * SAF * ABS * EF * ED}{BW * AT} * 10^{-6}$$

where C_{POE} is the exposure point concentration of mercury in soil (mg/kg); EF is the exposure frequency (150 day/year, a value suitable for a non-residential use). For the remaining parameters, recommend values [62–64] were used: R_{ing} is the ingestion rate (100 mg/day for adult, 200 mg/day for children); ED is the exposure duration (24 years for adults, 6 years for children); SA is the exposed skin area (5700 cm^2 for adults, 2800 cm^2 for children); SAF is the skin adherence factor (0.07 mg/cm^2 day for adults, 0.2 mg/cm^2 day for children); ABS is the dermal absorption factor (0.01 unitless); BW is the average body weight (70 kg for adults,15 kg for children); AT is the average time of exposure to non-carcinogens (ED × 365 day/year).

In case of inhalation pathways (vapor and dust), HQ (i.e., $HQ_{inhalation}$) was calculated by dividing the exposure concentration (EC, mg/m^3) to the reference toxicity concentration value (RfC, mg/m^3), rather than on the inhalation rate and average body weight:

$$HQ = \frac{EC}{RfC}$$

where RfC was set to 3.0×10^{-4} mg/m^3 [61] and EC was estimated as starting from the predicted concentration in air (mg/m^3), according to:

$$EC = \frac{C_{POE} * ET * EF * ED}{AT}$$

ET is the exposure time (3 h/day, suitable for a recreational area), AT is given by ED × 365 day/year × 24 h/day and C_{POE} is the concentration in air at the exposure point (mg/m^3) given by:

$$C_{POE} = C_S * FT$$

FT is the estimated transport factor and C_S is the concentration at the source of emission ($<C_{POE}$). FTs are obtained by mathematical models considering direction, rate, and extent of chemical migration, if the point of exposure for a receptor is not at the source. According to the ASTM standard [57], the transport model related to dust inhalation pathways is identified with the particle emission factor (V_{Fp}), while in the case vaporization of a compound from surface soil to outdoor air, the FT is the volatilization factor (VF_{SS}). Both V_{Fp} and VF_{SS}, predicting the attenuation of chemical concern away from the soil source, were calculated by using both the site-specific data (source geometry, vadose zone soil feature and metereological parameters) and physico-chemical properties obtained during field investigations, in addition to the conservative default values suggested by the ASTM standard: 7.42×10^{-7} and 4.60×10^{-12} (mg/m^3-air)/(mg/kg-soil), respectively.

The cumulative risk from simultaneous exposure to several non-carcinogens is defined by the screening level hazard index (HI) as:

$$HI = HQ_{ingestion} + HQ_{dermal} + HQ_{inhalation}$$

An HI value less than unity indicates that the risk is acceptable; otherwise, if HI exceeds one, non-carcinogenic effects are in danger of occurring, with probability increasing as the value of the HI increases.

4. Results

4.1. Soil and Plants

TOC, pH, trace element data and total Hg concentration in borehole samples, rhizosphere, and dandelion leaves are reported in Tables 1 and 2. The total organic carbon content ranged between 0.42 and 1.92 wt%. Samples from both boreholes and trenches were characterized by relatively high Fe, Mn, and Cr content (from 22 to 35 g/kg; from 495 to 1143 mg/kg; and from 76 to 129 mg/kg, respectively). Lead concentration in PZ1-A, PZ1-B, PZ2-A, T1-A, and T1-B exceeded the maximum concentration level (MCL) imposed by Italian regulations for residential and recreational areas (100 mg/kg). Cu and Zn exceeded the MCL (120 mg/kg and 150 mg/kg, respectively) in PZ1-A, T1-B, PZ2-A, and T1-B. It has to be noted that the Cr, Ni, and V contents overlapped with the concentration patterns that characterized the natural background of the Pisa plain sediments [65], interpreted as having originated from erosion and the weathering of ophiolitic rocks in the Serchio and Arno River Apennine catchments. Pb, Cu and Zn enrichments were not attributable to the Olocene sediments of the Pisa floodplain, and reflected inputs from anthropogenic sources such as the effects of urban vehicles [66]. Total mercury was above the MCL (1 mg/kg) in the borehole and trench samples (except PZ2-B), reaching 54 mg/kg; the Hg_T concentration in the PZ3 profile showed that Hg contamination was confined to the shallower soil layers. Mercury in the dandelion rhizosphere soil was widespread at concentrations exceeding MCL for almost the entire area, even if not homogeneously distributed, reaching 172 mg/kg. The Hg in dandelion leaves ranged between 0.42 and 1.50 mg/kg; no correlation with the Hg content in the rhizosphere was observed. The Hg content in the roots was between 0.01 and 0.03 mg/kg, indicating that the level of Hg uptake by plants from soil was minimal, or mercury does not reside in the roots. It is worth noting that leaves from dandelion plants growing in vases had comparable Hg content to the leaves of plants growing in the field. This suggests that the Hg uptake in leaves mainly comes from atmospheric mercury (e.g., [67]), most likely Hg^0. It is worth noting that the mercury vapor concentration during soil gas sampling obtained by suck-up techniques [68] reached 1300 ng/m^3, confirming that gaseous elemental mercury in soil has been spilled outside.

Table 1. TOC (wt%), pH, and trace element (mg/kg) analysis of soil, together with the maximum concentration level (MCL, mg/kg) imposed by Italian regulations for residential and recreational areas. Values exceeding the MCL are in bold.

	Boreholes				Trench		MCL *
	PZ-1A	PZ-1B	PZ-2A	PZ-2B	T1-A	T1-B	
TOC	0.98	0.96	1.28	0.42	1.92	0.68	
pH	8.4	8.4	8.3	8.4	8.2	8.3	
Li	37	40	27	30	43	35	
Be	1.59	1.76	1.16	1.15	1.79	1.49	2
Mn	940	980	785	495	1143	911	
Co	14.8	16.3	12.2	12.1	17.2	14.1	20
Ni	76	83	57	57	80	72	120
Cu	**124**	103	68	35	56	**149**	120
Zn	135	136	**266**	77	98	**163**	150
Sr	115	124	144	81	156	104	
Mo	0.5	0.5	0.5	<0.5	<0.5	<0.5	
Ag	0.67	0.85	0.64	0.12	1.26	0.82	
Sn	8.8	9.2	6.4	2.0	8.0	9.7	
Cd	0.27	0.28	0.34	0.11	0.17	0.38	2
Sb	0.77	0.63	0.49	0.24	0.43	0.72	10
Ba	213	213	320	130	209	210	
Tl	0.39	0.41	0.26	0.25	0.42	0.37	1
Pb	**113**	**127**	**136**	21	**189**	**124**	100
Th	6.7	7.0	5.5	5.7	7.3	6.6	
U	0.79	0.82	0.67	0.67	0.94	0.87	
V	70	77	50	50	78	66	90
Cr(tot)	107	129	76	76	115	106	150
Cr (VI)	<1	<1	<1	<1	<1	<1	2
Fe	33,035	35,463	21,994	23,523	34,749	30,510	
As	9.1	9.0	6.4	5.0	8.8	8.4	20
Se	1.3	1.4	1.1	1.1	2.9	2.6	3

* Legislative Decree No. 152/2006 approving the Code on the Environment.

Table 2. Hg concentration (mg/kg) in rhizosphere and Taraxacum officinale leaves, borehole and trench samples together with the sampling depth (m).

Boreholes	Sampling Depth	Hg	Taraxacum Officinale	Hg	Rhizosphere	Hg	Trench	Sampling Depth	Hg
PZ-1A	0.1–1	26.9	R1	0.62	R1	0.99	T1-A	0.1–0.5	3.9
PZ-1B	1.2–1.6	26.3	R2	0.42	R2	0.08	T1-B	1	40
PZ-2A	0.1–1	4.6	R3	0.85	R3	8.49			
PZ-2B	1.2–1.6	0.3	R4	0.26	R4	13.1			
PZ-3-1	0.31–0.34	26.8	R5	0.82	R5	75			
PZ-3-2	0.54–0.57	54.0	R6	0.95	R6	172			
PZ-3-3	0.82–0.85	1.19	R7	0.84	R7	3.21			
PZ-3-4	1.11–1.14	0.38	R8	1.17	R8	7.4			
PZ-3-5	1.31–1.34	0.55	R9	0.79	R9	3.33			
PZ-3-6	1.80–1.84	0.14	R10	0.11	R10	4.55			
PZ-3-7	2.22–2.24	0.07	R11	1.50	R11	24.9			
PZ-3-8	2.54–2.56	0.05	In vase	0.31					
PZ-3-9	2.79–2.81	0.09							

4.2. Hg Speciation in Soil

In order to quantify the Hg forms in soils, the PZ1-A and PZ2-A samples were chosen as the best representative of the area in terms of soil mercury contamination (Figure 2, Table 1).

4.2.1. Hg Determined by Chemical Extraction

The results of sequential extraction for PZ1-A and PZ2-A soils are graphically shown in Figure 3.
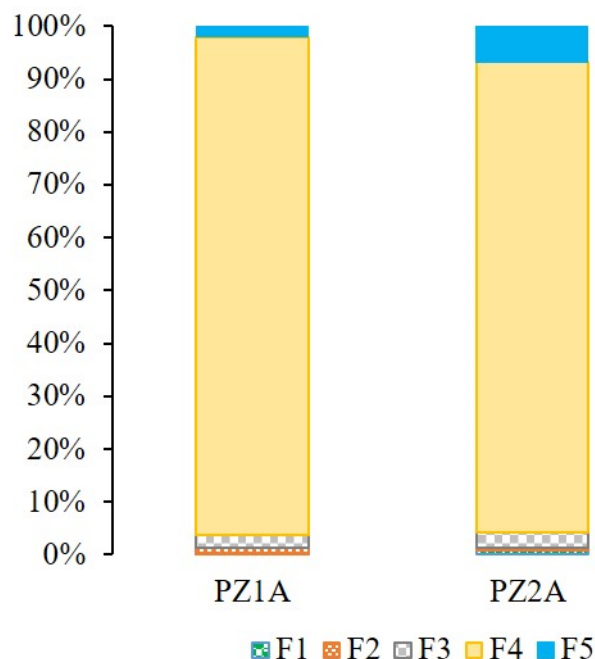

Figure 3. Normalized Hg F-fraction (wt%) extracted by each extractant solution for soil samples PZ1A and PZ2-A (F1 = distilled water, F2 = 0.01 M HCl + 0.1 M CH$_3$COOH, F3 = 1 M KOH, F4 = 12 M HNO$_3$, F5 = aqua regia).

The soil samples had similar distributions of Hg species, with the F4 fraction (12 M HNO$_3$ extractant) being the most abundant (79 ± 9%). This fraction was intended as a representative of both elemental mercury and mercury bound to Fe and Mn oxides. The F5 fraction (aqua regia extractant) revealed the possible occurrence of a minor amount of mercury sulfides (3.7 ± 2.6%) suggesting that, in general, conditions were not favorable to the spontaneous stabilization of mercury by conversion to cinnabar or metacinnabar. The F3 fraction (1 M KOH extractant), representing organo-chelated Hg, was 2.6 ± 1.1%, suggesting a minor fraction of Hg associated with soil organic matter. The Hg sequential extraction experiments also revealed that the F1 fraction (distilled water) and F2 fraction (0.01 M HCl + 0.1 M CH$_3$COOH) extracted a negligible amount of mercury from the soil (0.4 ± 0.3% and 0.2 ± 0.2%, respectively).

Methylmercury from ingestion and inhalation pathways easily enter the bloodstream and rapidly distribute to all tissues, accumulating in the brain. The presence of methylmercury in soil is hence of particular importance in characterizing mercury hazard. The extraction results indicated very low values of methylmercury species in the studied soil. In particular, the measured MeHg concentrations of the PZ1-A and PZ2-A samples corresponded to 0.1%, respectively, of total Hg content.

4.2.2. Hg Thermal Desorption Analysis

Considering the comparable results obtained during the sequential chemical extraction for PZ1-A and PZ2-A soils, thermo-desorption experiments at different heating rates were applied only to the PZ1-A sample. The obtained thermograms had the same shape and were fitted by two peaks ranging between 110–130 °C (peak #1) and 160–200 °C (peak #2) in experiments at variable heating rates. An example is shown in Figure 4.
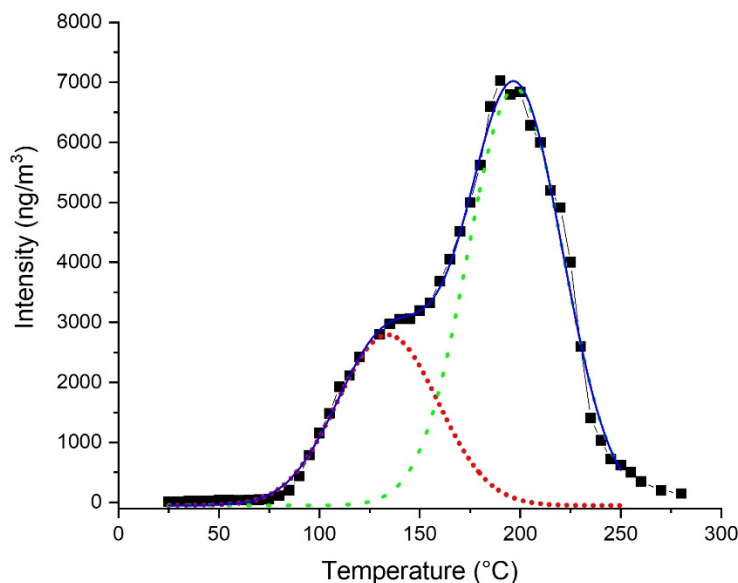
Figure 4. Example of thermo-desorption curve for PZ1-A soil sample (black squares). Deconvolution (blue line) indicates the occurrence of peaks centered at $133 \pm 2\,^{\circ}$C (red dot, peak #1) and $197.4 \pm 0.9\,^{\circ}$C (green short dash, peak #2). R-square = 0.99.

Peak #1 is attributable to the desorption of Hg^0 free in the soil matrix [69]. In order to assign the peak #2 to Hg species, activation energy was obtained by thermo-release curves measured at the heating rates (β) of 8, 10, 12, 20, 35 $^{\circ}$C/min. As expected, the peak maximum (T_{peak}) shifted to a higher temperature with increasing β [70,71]. T_{peak} and β can be used to determine the first-order activation energy (E_a) of Hg vapor emission from soil according to:

$$\ln\left(\frac{T_{peak}^2}{\beta}\right) = \frac{E_a}{RT_{peak}} + \ln\left(\frac{E_a}{AR}\right)$$

where A represents the Arrhenius pre-exponential factor and R the Boltzmann gas constant [71]. In a series of heating experiments with different β a linear correlation is hence expected between T_{peak}^2/β and $1/T_{peak}$, whose slope is given by E_a/R. The results obtained for PZ1-A soil are graphically shown in Figure 5.
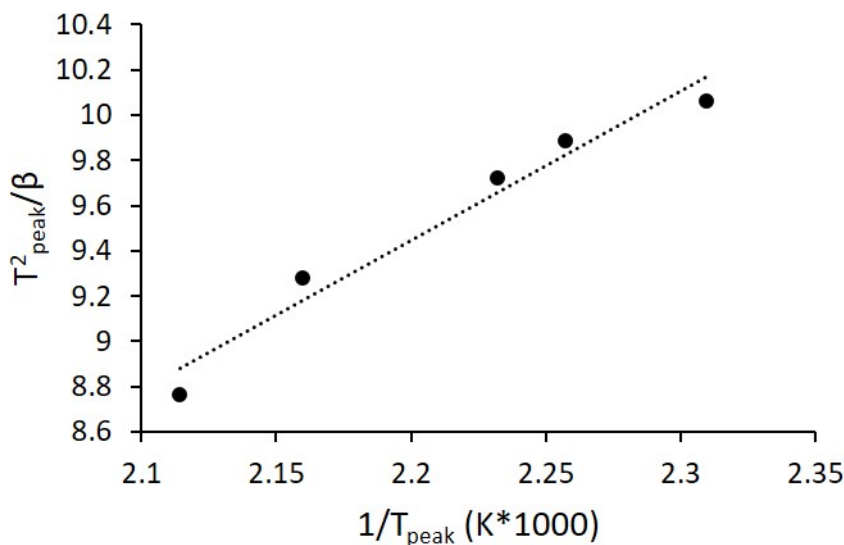
Figure 5. T_{peak}^2/β vs. $1/T_{peak}$ (T in K) diagram. The slope of the linear fitting (dotted line) gives the activation energy (E_a/R). R-square = 0.96.

The slope of the regression (6.60) gives an activation energy of 13.2 Kcal/mol. A range of desorption activation energies have been reported for Hg gas emission from soils, mostly depending on the physico-chemical properties of the soil and sorption processes [72–75]. The E_a obtained in this study was close to the enthalpy of the $Hg^0_{liq} \rightarrow Hg^0_{gas}$ reaction (about 14 Kcal/mol), and might reflect the vaporization of elemental Hg more deeply retained within the soil structure, compared with that represented by peak #1. Indeed, a double peak for Hg^0 release with a maximum at approximately 100 °C and 200 °C has been reported in the literature (e.g., [76]) and ascribed to Hg^0 as variably bound to Fe oxydydroxides, while a higher desorption temperature (200–300 °C) is attributed to matrix bound Hg^{2+} [69,77,78].

There is no clear consensus about this matter; however, considering the obtained E_a we can assign peak #2 to matrix-bound Hg^0, where the matrix is a mineral phase. Most of the Hg^{2+} released during the pristine contamination would hence have been reduced to Hg^0. Indeed, in natural settings, divalent mercury can be reduced to elemental mercury by specific inorganic reducing agents, such as bacteria and sunlight; the process of the biotic and abiotic production of elemental mercury in the soil–water system via Hg^{2+} reduction represents a pathway in the biogeochemical cycle of mercury. Furthermore, experimental studies have demonstrated that the ferrous iron associated with iron oxyhydroxides, such as magnetite grains commonly found in the Pisa plain sediments [52] and other minerals (e.g., siderite), is a reductant of Hg^{2+}, with the formation of elemental Hg^0 by surface reactions (e.g., [79]).

The deconvolution of the desorption curve, scaled to the % recovery in the F4 fraction obtained by chemical sequential extraction, yielded that about 25% of total mercury in soil was free Hg^0 (peak #1) and 55% was matrix-bound Hg^0 (peak #2). It is worth mentioning that cinnabar and/or metacinnabar, released at higher temperature and highlighted by sequential extraction, were not detected by thermograms, suggesting that their amount was below the peak resolution.

4.3. Water

Physico-chemical parameters, major ions, and trace element content of groundwater are reported in Table 3. In PZ1_W and PZ2_W temperature was quite constant in both the summer and winter surveys (between 15.4 and 17.3 °C), despite large changes in the air temperature. Water had a circum-neutral pH, and electrical conductivity was somewhat lower during the dry season (July 2019; EC = 1955–2230 μS/cm) compared with the wet season (January 2020; EC = 2600–3370 μS/cm). Dissolved oxygen ranged between 2.0 and 3.6 mg/L, indicating that the original oxygen content was significantly modified through chemical and biological processes. In particular, the occurrence of NH_4^+ might reflect the decay of buried organic matter; indeed, at the Eh-pH conditions measured in groundwater, NH_4^+ oxidized to nitrate–nitrogen, suggesting the occurrence of water bodies in the aquitard of anoxic conditions not directly sampled during the surveys. The major ion chemistry indicated that PZ1_W and PZ2_W belonged to Na-Cl-type water, according to the classification based on the Piper diagram (Figure 6). The relatively high Na and Cl content indicated the contribution of a marine component. However, the SO_4^{2-} content was lower compared with what was expected on the basis of the Cl^-/SO_4^{2-} ratio in seawater, pointing to sulfate reduction by organic matter. This hypothesis was supported by the H_2S "rotten egg" smell and the relatively high HCO_3^- content measured. The seasonal reducing environment, occurring in soil as a result of the different hydrogeochemical conditions and sulfate reduction by sulfate-reducing microbes, might locally facilitate the formation of minor amounts HgS from elemental mercury [80].

Groundwater was characterized by high Mn, relatively high Fe content, and in some cases Ni above MCL (50, 200 and 20 μg/L for Mn, Fe and Ni, respectively), as expected on the basis of the lithology of the aquitard originating from the erosion of ophiolitic rock outcropping in the Apennine catchments, and commonly found in groundwater in the coastal plain of Pisa. Arsenic in PZ1_W1 slightly exceeded the MCL (10 μg/L),

possibly reflecting As hosted in sulfide veins related to the hydrothermal activity across the northern Apennine ophiolites. With the exception of Mn, Ni, and As in PZ1_W1, the concentrations of potentially toxic elements were below the corresponding MCL imposed by Italian regulations. It is worth noting that Hg was below the detection limit of 0.2 µg/L in all water samples.

Table 3. Physico-chemical parameters, concentration of major ions and trace elements in groundwater from PZ1 and PZ2 piezometers collected in July 2019 (samples PZ1_W1 and PZ2_W1) and January 2020 (samples PZ1_W2 and PZ2_W2) together with the maximum concentration levels (MCL, mg/kg) imposed by Italian regulations for groundwater. Values exceeding the MCL are in bold.

Sample	PZ1-W1 July 2019	PZ1-W2 January 2020	PZ2-W1 July 2019	PZ2-W2 January 2020	MCL *
T_{water} (C°)	17.3	15.5	15.7	15.4	
T_{air} (C°)	29.6	10.5	28.5	11.8	
pH	7	7.2	7.1	7.2	
EC	1955	2600	2230	3370	
DO (mg/l)	2.1	3	3.6	2	
Eh (V)	0.17	0.28	0.22	0.42	
NH_4^+ (mg/L)		1.59		2.1	
Hg (µg/L)	<0.2	<0.2	<0.2	<0.2	1
Na^+ (mg/L)	296	299	353	337	
K^+ (mg/L)	8.3	7.4	16	17	
Mg^{2+} (mg/L)	57	58	60	66	
Ca^{2+} (mg/L)	231	247	208	240	
F^- (mg/L)	<1.5	<1.5	<1.5	<1.5	1.5
Cl^- (mg/L)	485	516	578	668	
NO_3^- (mg/L)	<10	<10	<10	<10	50
SO_4^{2-} (mg/L)	96	119	147	194	250
HCO_3^- (mg/L)	799	927	653	683	
Li (µg/L)	10.3	7.7	11.6	8.2	
Be (µg/L)	<0.07	<0.1	<0.07	<0.1	4
Mn (µg/L)	**4949**	**4082**	**2454**	**3404**	50
Co (µg/L)	8.2	2.88	4.1	4.16	50
Ni (µg/L)	**43**	**23.4**	**26.3**	**30**	20
Cu (µg/L)	<22	26	<22	23	1000
Zn (µg/L)	<70	<70	<70	<70	3000
Sr (µg/L)	1882	1779	1644	1874	
Mo (µg/L)	3.7	2.38	3.5	2.37	
Sn (µg/L)	<0.9	<0.9	<0.9	<0.9	
Cd (µg/L)	<0.08	<0.08	<0.08	<0.08	5
Sb (µg/L)	0.56	<0.4	<0.4	<0.4	5
Ba (µg/L)	356	277	404	376	
Tl (µg/L)	<0.07	<0.06	<0.07	<0.06	2
Pb (µg/L)	<2	<2	<2	<2	10
U (µg/L)	2.26	1.74	3.29	2.88	
V (µg/L)	1.19	<1	<1	<1	
Cr (µg/L)	<1	<1	<1	<1	50
Fe (µg/L)	**5520**	**5698**	**842**	134	200
As (µg/L)	**12.3**	9.7	3.7	1.68	10

* Legislative Decree No. 152/2006 approving the Code on the Environment.

4.4. Risk Analysis

Non-carcinogenic health risk assessment was performed by calculating HQ and HI. The data obtained using the highest mercury concentration measured on site (172 mg/kg) and speciation results (percent yields of 3.7, 25, 55 and 0.1 for mercury sulfide, free Hg^0, matrix-bound Hg^0 and methylmercury, respectively; see Section 4.2) are shown in Table 4.
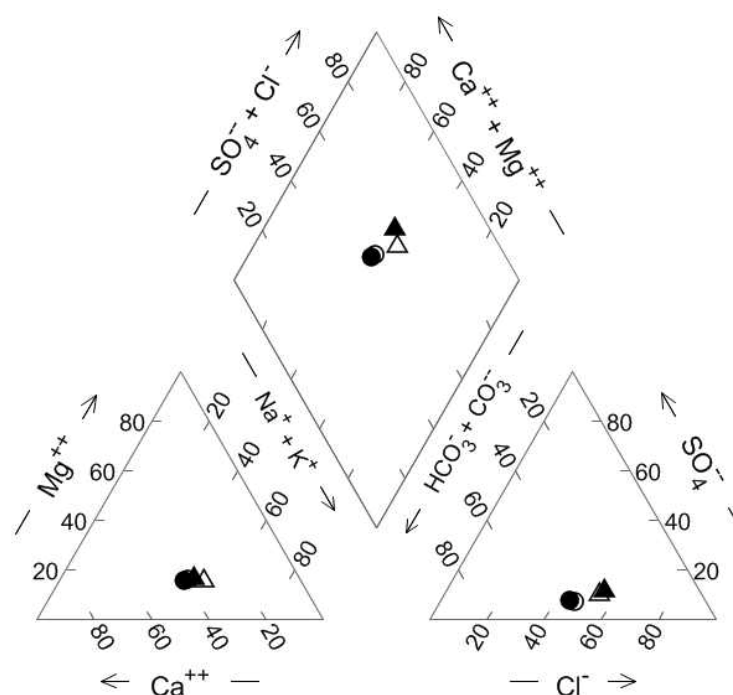
Figure 6. Piper diagram for the studied groundwater samples. Symbols: circle, PZ1; triangle: PZ2. Open and filled symbols refer to July 2019 (W1) and January 2020 (W2) samplings, respectively.

Table 4. Summary of Hazard Quozient (HQ) for non-carcinogenic risk calculated for different exposure routes for children and adult receptors (values for adults when different are in brackets) based on mercury maximum concentration and speciation data (see text).

HQ	Soil Ingestion	Dermal Contact	Inhalation Vapor	Inhalation Dust
Free Hg^0 $RfD_{ing} = 1.6 \times 10^{-4}$ mg/kg/day $RfC = 3 \times 10^{-4}$ mg/m^3	1.47 (0.16)	4.12×10^{-2} (6.30×10^{-3})	5.46×10^{-3}	3.39×10^{-8}
Matrix-bound Hg^0 $RfD_{ing} = 1.6 \times 10^{-4}$ mg/kg/day	3.24 (0.35)	9.07×10^{-2} (1.38×10^{-2})	-	7.45×10^{-8}
Mercury sulfide $RfD_{ing} = 3 \times 10^{-4}$ mg/kg/day	0.12 (1.24×10^{-2})	3.25×10^{-3} (4.97×10^{-4})	-	*
Methylmercury $RfD_{ing} = 10^{-4}$ mg/kg/day	9.42×10^{-3} (1.01×10^{-3})	2.64×10^{-4} (4.03×10^{-5})	-	*
Sum of individual hazard quotients	4.84 (0.52)	0.14 (2.06×10^{-2})	5.46×10^{-3}	1.08×10^{-8}

* RfC not available.

It was observed that the risk was associated with soil ingestion by children, while dermal contact and inhalation pathways did not produce a significant health risk. In particular, an $HQ_{ingestion}$ exceeding unit was obtained for children for the cases of free and matrix-bound Hg^0 (HQ of 1.47 and 3.24, respectively), while for sulfide-bound Hg and methylmercury the HQ value is negligible.

The hazard index calculated considering all the exposure routes active on-site exceeded unity (HI = 4.99), and therefore posed a (non-cancerous) risk to children, who represent the major target users of the playground space, and the most vulnerable group of city residents.

It is worth mentioning that the speciation data obtained in this study allowed us to perform an actual risk assessment instead of using the total Hg concentration for each exposure pathway, with the latter leading to an overestimation of the risk.

5. Discussion

The measured metal concentrations revealed that soil samples in the studied urban green space—planned to be converted into a recreational area in the town of Pisa—comprised potentially toxic elements. The major threat was related to the occurrence of

mercury, largely exceeding the guideline concentration values for residential use imposed by Italian regulations. Mercury in the soil was not attributable to lithogenic sources, representing the legacy of $HgCl_2$ applied in the past artisanal tannery activities that characterized the site. The data showed that mercury contamination was widespread, with the highest concentration, reaching 172 mg/kg, measured in the rhizosphere.

The analytical results from soil gas sampling revealed that mercury degassing is an active process on the site, in agreement with the results obtained by the thermal desorption laboratory experiments demonstrating the occurrence of free Hg^0 and Hg^0 retained in the soil, produced by reducible matrix-bound Hg^{2+}. Furthermore, the sequential chemical extraction indicated that the main Hg species in soil were extracted by the 12 M HNO_3 fraction, representative of both elemental and matrix-bound Hg. We can suppose that the matrix-bound Hg mostly comprised Hg adsorbed in the mineral surface, in particular onto Fe-Mn oxyhydroxides commonly found in the Pisa alluvial plain. The relatively high pH of the soil may have enhanced the Fe-Mn oxyhydroxides' sorptive capacity [81].

The chemical sequential extraction also indicated that the organo-chelated Hg fraction was below 3 wt%. A minor amount of mercury (below 4 wt% from the sequential extraction results) had possibly formed sulfides. Indeed, in anaerobic Hg-contaminated soils, the microbial reduction of sulfate can lead to the in situ formation of mercuric sulfide (HgS), occurring as cinnabar or metacinnabar.

The obtained results hence highlight that Hg^{2+} from the original industrial input of mercuric chloride has mostly undergone reduction—therefore being less toxic to the environment and comprising less reactive Hg^0—but is still highly toxic to humans when inhaled [82], heterogeneously distributed, and variably bound to the soil matrix. The microbial reduction of Hg^{2+} to Hg^0 has been documented in periodically flooded anaerobic soils, such as the site under study during heavy raining events [83]. Reduction reactions in surface soils may also be enhanced photochemically [84].

Mercury contamination has not been detected in groundwater, indicating that Hg^{2+} reduction does not lead to the release of a significant amount of Hg in solution. This is interpreted as reflecting soil speciation, revealing the occurrence of insoluble HgS in soil, stable organo-chelated Hg complexes, and Hg^0 having relatively low solubility (about 6.0×10^{-5} g/L at 25 °C). This was also confirmed by water leachates during the sequential extraction experiments (F1 fraction), which contained negligible amounts of mercury. It should also be noted that the water table level in the study area was generally not sufficiently high enough to be in contact with the contaminated soil layer, preventing the direct scavenging of Hg from groundwater. In addition, in the case of Hg release to groundwater, lateral fluxes in the aquitard would be limited due to the low hydraulic conductivity, reducing the possibility of soluble Hg migration pathways. Even though, on the basis of the available data, there is no evidence that Hg enters the groundwater, the observed increase in the Cl^- concentration might result in forming stable aqueous complexes with Hg, enhancing mercury leaching during the interaction between groundwater and the mercury mineral phases occurring at depth [85]. Indeed, the redox profile in the aquifer and the dynamic between infiltrating rainwater and deeper saltwater lenses may favor Hg-Cl complexes, promoting the possible dissolution of Hg-bearing sulfides. This requires the monitoring of groundwater to be continued.

6. Conclusions

The re-use of dismissed areas by urban greening policies represents an effective way of improving the quality of life for citizens, and therefore has an important social function. In the present study, the soil and groundwater quality of an abandoned site in the city center of Pisa, planned to become a new public green space, was investigated by geochemical analysis. The obtained results highlighted that mercury contamination in the soil is the major threat. According to historical records, this mercury contamination represents the legacy of a past artisanal tannery that used $HgCl_2$ in leather processing. The activity ceased without a reclamation program, and specific monitoring and management were

not carried out. The data indicate that Hg contamination is widespread, but confined to the uppermost soil layers, and that this contaminant is not mobilized to groundwater. Soil chemical sequential extraction, thermal desorption experiments, and field measurements indicated that redox conversion of Hg^{2+} into Hg^0 occurred in the soil, and that Hg^0 was heterogeneously distributed and variably bound to the soil matrix. A small fraction of mercury was likely fixed in soil as HgS. Even if elemental mercury was less reactive and less toxic to the environment with respect to Hg^{2+} and organomercurials, the risk assessment based on the speciation data indicates an unacceptable risk (HI > 1) due to the possible direct soil ingestion of children. This study demonstrates the usefulness of a site-specific investigation approach providing geochemical data for modelling the risks associated with human exposure to hazardous elements in an urban environment—in this instance mercury. Furthermore, risk assessments should be the main basis for remedial action regarding human health protection.

Author Contributions: Conceptualization, R.P. and L.G.; methodology, R.G. and M.B.; software, S.A. and M.B.; validation, L.G., R.P. and S.A.; formal analysis, L.G. and M.V.; investigation, L.G., M.V., R.P. and R.G.; writing—original draft preparation, R.P. and L.G.; writing—review and editing, L.G. and R.P.; visualization, L.G.; supervision, R.P.; project administration, R.P. All authors have read and agreed to the published version of the manuscript.

Institutional Review Board Statement: Not applicable.

Informed Consent Statement: Not applicable.

Conflicts of Interest: The authors declare no conflict of interest.

References

1. Beckers, F.; Rinklebe, J. Cycling of mercury in the environment: Sources, fate, and human health implications: A review. *Crit. Rev. Environ. Sci. Technol.* **2017**, *47*, 693–794. [CrossRef]
2. Bernhoft, R.A. Mercury Toxicity and Treatment: A Review of the Literature. *J. Environ. Public. Health* **2012**, *2012*, 460508. [CrossRef] [PubMed]
3. Rice, K.M.; Walker, J.E.M.; Wu, M.; Gillette, C.; Blough, E.R. Environmental mercury and its toxic effects. *J. Prev. Med. Public Health* **2014**, *47*, 74–83. [CrossRef] [PubMed]
4. Tariq, M. Toxicity of mercury in humans: A review. *J. Clin. Toxicol.* **2019**, *9*, 431.
5. WHO. *Ten Chemicals of Major Health Concern*; World Health Organization: Geneva, Switzerland, 2017.
6. Ceccatelli, S.; Aschner, M. *Methylmercury and Neurotoxicity*; Springer: New York, NY, USA, 2012. [CrossRef]
7. Evers, D.C.; Keane, S.E.; Basu, N.; Buck, D. Evaluating the effectiveness of the Minamata Convention on Mercury: Principles and recommendations for next steps. *Sci. Total Environ.* **2016**, *569–570*, 888–903. [CrossRef] [PubMed]
8. Selin, N.E. Global biogeochemical cycling of mercury: A review. *Annu. Rev. Environ. Resour.* **2009**, *34*, 43–63. [CrossRef]
9. Wang, Y.; Liu, G.; Li, Y.; Liu, Y.; Guo, Y.; Shi, J.; Hu, L.; Cai, Y.; Yin, Y.; Jiang, G. Occurrence of mercurous [Hg(I)] species in environmental solid matrices as probed by mild 2-mercaptoethanol extraction and HPLC-ICP-MS analysis. *Environ. Sci. Technol. Lett.* **2020**, *7*, 482–488. [CrossRef]
10. Gilmour, C.C.; Podar, M.; Bullock, A.L.; Graham, A.M.; Brown, S.D.; Somenahally, A.C.; Johs, A.; Hurt, R.A., Jr.; Bailey, K.L.; Elias, D.A. Mercury methylation by novel microorganisms from new environments. *Environ. Sci. Technol.* **2013**, *47*, 11810–11820. [CrossRef]
11. Celo, V.; Lean, D.R.S.; Scott, S.L. Abiotic methylation of mercury in the aquatic environment. *Sci. Total Environ.* **2006**, *368*, 126–137. [CrossRef]
12. Compeau, G.C.; Bartha, R. Sulfate-reducing bacteria: Principal methylators of mercury in anoxic estuarine sediment. *Appl. Environ. Microbiol.* **1985**, *50*, 498–502. [CrossRef]
13. Shao, D.; Kang, Y.; Wu, S.; Wong, M.H. Effects of sulfate reducing bacteria and sulfate concentrations on mercury methylation in freshwater sediments. *Sci. Total Environ.* **2012**, *424*, 331–336. [CrossRef] [PubMed]
14. Achá, D.; Hintelmann, H.; Yee, J. Importance of sulfate reducing bacteria in mercury methylation and demethylation in periphyton from Bolivian Amazon region. *Chemosphere* **2011**, *82*, 911–916. [CrossRef] [PubMed]
15. Horvat, M.; Covelli, S.; Faganeli, J.; Logar, M.; Mandić, V.; Rajar, R.; Širca, A.; Žagar, D. Mercury in contaminated coastal environments; a case study: The Gulf of Trieste. *Sci. Total Environ.* **1999**, *237–238*, 43–56. [CrossRef]
16. Gosnell, K.; Balcom, P.; Ortiz, V.; DiMento, B.; Schartup, A.; Greene, R.; Mason, R. Seasonal cycling and transport of mercury and methylmercury in the turbidity maximum of the Delaware Estuary. *Aquat. Geochem.* **2016**, *22*, 313–336. [CrossRef]

17. King, J.K.; Kostka, J.E.; Frischer, M.E.; Saunders, F.M. Sulfate-reducing bacteria methylate mercury at variable rates in pure culture and in marine sediments. *Appl. Environ. Microbiol.* **2000**, *66*, 2430–2437. [CrossRef]

18. Leopold, K.; Foulkes, M.; Worsfold, P.J. Methods for the determination and speciation of mercury in natural waters. A review. *Anal. Chim. Acta* **2010**, *663*, 127–138. [CrossRef]

19. Mendes, L.A.; de Lena, J.C.; do Valle, C.M.; Fleming, P.M.; Windmöller, C.C. Quantification of methylmercury and geochemistry of mercury in sediments from a contaminated area of Descoberto (MG), Brazil. *Appl. Geochem.* **2016**, *75*, 32–43. [CrossRef]

20. Ullrich, S.M.; Ilyushchenko, M.A.; Uskov, G.A.; Tanton, T.W. Mercury distribution and transport in a contaminate driver system in Kazakhstan and associated impacts on aquatic biota. *Appl. Geochem.* **2007**, *22*, 2706–2734. [CrossRef]

21. Hammerschmidt, C.R.; Fitzgerald, W.F. Geochemical controls on the production and distribution of methylmercury in near-shore marine sediments. *Environ. Sci. Technol.* **2004**, *38*, 1487–1495. [CrossRef]

22. Schaefer, J.K.; Morel, F.M.M. High methylation rates of mercury bound to cysteine by *Geobacter sulfurreducens*. *Nat. Geosci.* **2009**, *2*, 123–126. [CrossRef]

23. Benoit, J.M.; Gilmour, C.C.; Heyes, A.; Mason, R.P.; Miller, C.L. Geochemical and biological controls over methylmercury production and degradation in aquatic ecosystems. *ACS Symp. Ser.* **2003**, *835*, 262–297.

24. Liu, Y.; Zhi, L.; Shaoqi, Z.; Feng, X. Effects of mercury binding by humic acid and humic acid resistance on mercury stress in rice plants under high Hg/humic acid concentration ratios. *Environ. Sci. Pollut. Res.* **2020**, *27*, 18650–18660. [CrossRef] [PubMed]

25. Skyllberg, U.; Bloom, P.R.; Qian, J.; Lin, C.-M.; Bleam, W.F. Complexation of mercury(II) in soil organic matter: EXAFS evidence for linear two-coordination with reduced sulfur groups. *Environ. Sci. Technol.* **2006**, *40*, 4174–4180. [CrossRef] [PubMed]

26. Thanabalasingam, P.; Pickering, W.F. The sorption of mercury(II) by humic acids. *Environ. Pollut.* **1985**, *9*, 267–279. [CrossRef]

27. Zhang, J.; Dai, J.; Wang, R.; Li, F.; Wang, W. Adsorption and desorption of divalent mercury (Hg2+) on humic acids and fulvic acids extracted from typical soils in China. *Colloids Surf. A Physicochem. Eng. Asp.* **2009**, *335*, 194–201. [CrossRef]

28. Bonnissel-Gissinger, P.; Alnot, M.; Lickes, J.-P.; Ehrhardt, J.-J.; Behra, P. Modeling the adsorption of mercury(II) on (hydr)oxides II: A-FeOOH (goethite) and amorphous silica. *J. Colloid Interface Sci.* **1999**, *215*, 313–322. [CrossRef]

29. Richard, J.-H.; Bishoff, C.; Ahrens, C.G.M.; Biester, H. Mercury (II) reduction and co-precipitation of metallic mercury on hydrous ferric oxide in contaminated groundwater. *Sci. Total Environ.* **2016**, *539*, 36–44. [CrossRef]

30. Ha, J.; Zhao, X.; Yu, R.; Barkay, T.; Yee, N. Hg(II) reduction by siderite ($FeCO_3$). *Appl. Geochem.* **2017**, *78*, 211–218. [CrossRef]

31. O'Loughlin, E.J.; Kelly, S.D.; Kemner, K.M.; Csencsits, R.; Cook, R.E. Reduction of Ag(I), Au(III), Cu(II), and Hg(II) by Fe(II)/Fe(III) hydroxysulfate green rust. *Chemosphere* **2003**, *53*, 437–446. [CrossRef]

32. O'Loughlin, E.J.; Boyanov, M.I.; Kemmer, K.M.; Thalhammer, K.O. Reduction of Hg(II) by Fe(II)-bearing spectate clay minerals. *Minerals* **2020**, *10*, 1079. [CrossRef]

33. Pannu, R.; Siciliano, S.D.; O'Driscoll, N.J. Quantifying the effects of soil temperature, moisture and sterilization on elemental mercury formation in boreal soils. *Environ. Pollut.* **2014**, *193*, 138–146. [CrossRef] [PubMed]

34. Rocha, J.C.; Sargentini, E., Jr.; Zara, L.F.; Rosa, A.H.; dos Santos, A.; Burba, P. Reduction of mercury(II) by tropical river humic substances (Rio Negro)—A possible process of the mercury cycle in Brazil. *Talanta* **2000**, *53*, 551–559. [CrossRef]

35. Wiatrowski, H.A.; Das, S.; Kukkadapu, R.; Ilton, E.S.; Barkay, T.; Yee, N. Reduction of Hg(II) to Hg(0) by magnetite. *Environ. Sci. Technol.* **2009**, *43*, 5307–5313. [CrossRef]

36. Zhang, T.; Kim, B.; Leyard, C.; Reinsch, B.C.; Lowry, G.V.; Deshusses, M.A.; Hsu-Kim, H. Methylation of Mercury by Bacteria Exposed to Dissolved, Nanoparticulate, and Microparticulate Mercuric Sulfides. *Environ. Sci. Technol.* **2012**, *46*, 6950–6958. [CrossRef] [PubMed]

37. Gibičar, D.; Horvat, M.; Logar, M.; Fajon, V.; Falnoga, I.; Ferrara, R.; Lanzillotta, E.; Ceccarini, C.; Mazzolai, B.; Denby, B.; et al. Human exposure to mercury in the vicinity of a chlor-alkali plant. *Environ. Res.* **2009**, *109*, 355–367. [CrossRef] [PubMed]

38. Wang, F.Y.; Wang, S.X.; Zhang, L.; Yang, H.; Wu, Q.R.; Hao, J.M. Characteristics of mercury cycling in the cement production process. *J. Hazard. Mater.* **2016**, *302*, 27–35. [CrossRef]

39. Wang, F.Y.; Wang, S.X.; Zhang, L.; Yang, H.; Gao, W.; Wu, Q.R.; Hao, J.M. Mercury mass flow in iron and steel production process and its implications for mercury emission control. *J. Environ. Sci.* **2016**, *43*, 293–301. [CrossRef]

40. Zhao, S.; Pudasainee, D.; Duan, Y.; Gupta, R.; Liu, M.; Lu, J. A review on mercury in coal compustion process: Content and occurrence forms in coal, transformation, sampling methods, emission and control technologies. *Prog. Energy Combust. Sci.* **2019**, *73*, 26–64. [CrossRef]

41. Covelli, S.; Langone, L.; Acquavita, A.; Piani, R.; Emili, A. Historical flux of mercury associated with mining and industrial sources in the Marano and Grado Lagoon (northern Adriatic Sea). *Estuar. Coast. Shelf Sci.* **2012**, *113*, 7–19. [CrossRef]

42. Vaselli, O.; Nisi, B.; Rappuoli, D.; Cabassi, J.; Tassi, F. Gaseous elemental mercury and total and leached mercury in building materials from the former Hg-mining area of Abbadia San Salvatore (Central Italy). *Int. J. Environ. Res. Public Health* **2017**, *14*, 425. [CrossRef]

43. Veiga, M.M.; Maxson, P.A.; Hylander, L.D. Origin and consumption of mercury in a small-scale gold mining. *J. Clean. Prod.* **2006**, *14*, 436–447. [CrossRef]

44. Mojammal, A.H.M.; Back, S.-K.; Seo, Y.-C.; Kim, J.-H. Mass balance and behavior of mercury in oil refinery facilities. *Atmos. Pollut. Res.* **2019**, *10*, 145–151. [CrossRef]

45. Krishnamoorthy, G.; Sadulla, S.; Sehgal, P.K.; Mandal, B.A. Greener approach to leather tanning process: D-Lysine aldehyde as novel tanninh agent for chrome-fre tanning. *J. Clean. Prod.* **2013**, *42*, 277–286. [CrossRef]

46. Tasca, A.L.; Puccini, M. Leather tanning:life cycle assessment of retanning, fatliquoring and dyeing. *J. Clean. Prod.* **2019**, *226*, 720–729. [CrossRef]

47. Reis, A.T.; Davidson, C.M.; Vale, C.; Pereira, E. Overview and challenges of mercury fractionation and speciation in soils. *TrAC Trends Anal. Chem.* **2016**, *82*, 109–117. [CrossRef]

48. Issaro, N.; Abi-Ghanem, C.; Bermond, A. Fractionation studies of mercury in soils and sediments: A review of the chemical reagents used for mercury extraction. *Anal. Chim. Acta* **2009**, *631*, 1–12. [CrossRef]

49. Bini, M.; Pappalardo, M.; Rossi, V.; Noti, V.; Amorosi, A.; Sarti, G. Deciphering the effects of human activity on urban areas through morphostratigraphic analysis: The case of Pisa, Northwest Italy. *Geoarchaeology* **2018**, *33*, 43–51. [CrossRef]

50. Bini, M.; Rossi, V.; Amorosi, A.; Pappalardo, M.; Sarti, G.; Noti, V.; Capitani, M.; Fabiani, F.; Gualandi, M.L. Palaeoenvironments and palaeotopography of a multilayered city during the Etruscan and Roman periods: Early interaction of fluvial processes and urban growth at Pisa (Tuscany, Italy). *J. Archeol. Sci.* **2015**, *59*, 197–210. [CrossRef]

51. Sarti, G.; Rossi, V.; Amorosi, A.; Bini, M.; Giacomelli, S.; Pappalardo, M.; Ribecai, C.; Ribolini, A.; Sammartino, I. Climatic signature of two mid-late Holocene fluvial incisions formed under sea-level highstand conditions (Pisa coastal plain, NW Tuscany, Italy). *Palaeogeogr. Palaeoclimatol. Palaeoecol.* **2015**, *424*, 183–195. [CrossRef]

52. Amorosi, A.; Rossi, V.; Sarti, G.; Mattei, R. Coalescent valley fills from the late Quaternary record of Tuscany (Italy). *Quat. Int.* **2013**, *288*, 129–138. [CrossRef]

53. Hojdová, M.; Rohovec, J.; Chrastný, V.; Penížek, V. The influence of sample drying procedures on mercury concentrations analyzed in soils. *Bull. Environ. Contam. Toxicol.* **2015**, *94*, 570–576. [CrossRef] [PubMed]

54. ISO 10390. *Soil Quality—Determination of pH*; International Organization for Standardization: Geneva, Switzerland, 2005.

55. Bloom, N.S.; Preus, E.; Katon, J.; Hiltner, M. Selective extractions to assess the biogeochemically relevant fractionation of inorganic mercury in sediments and soils. *Anal. Chim. Acta* **2003**, *479*, 233–248. [CrossRef]

56. Boszke, L.; Kowalski, A.; Astel, A.; Barański, A.; Qworek, B.; Siepak, J. Mercury mobility and bioavailability in soil from contaminated area. *Environ. Geol.* **2008**, *55*, 1075–1087. [CrossRef]

57. ASTM. *Standard Provisional Guide for Risk-Based Corrective Action*; Report E 2081-00; American Society for Testing Materials: West Conshohocken, PA, USA, 2000.

58. US EPA. *Soil Screening Guidance: Technical Background Document*; EPA/540/R-95/128; Office of Emergency and Remedial Response, US Environmental Protection Agency: Washington, DC, USA, 1996.

59. OEHHA. Technical Supporting Document for Noncancer RELs, Appendix D1 2008 (Updated July 2014). Available online: http://oehha.ca.gov/chemicals/mercury-inorganic (accessed on 9 February 2022).

60. USDoE. RAIS: Risk Assessment Information System. 2010. Available online: http://rais.ornl.gov (accessed on 9 February 2022).

61. US EPA. *Regional Screening level (RSLs)—User's Guide*; US Environmental Protection Agency: Washington, DC, USA, 2021.

62. USTCEQ. Texas Commission of Environmental Quality 2021. Current PCL Tables. Available online: www.tceq.texas.gov/remediation/trrp/trrppcls.html (accessed on 9 February 2022).

63. US EPA. *Risk Assessment Guidance for Superfund—Volume I: Human Health Evaluation Manual. Part A*; EPA/540/1-89/002; Office of Emergency and Temediation Response, US Environmental Protection Agency: Washington, DC, USA, 1989.

64. US EPA. Supplemental Guidance for Developing Soil Screening Levels for Superfund Sites. In *Solid Waste and Remedial Response*; OSWER 9355.4-24; US Environmental Protection Agency: Washington, DC, USA, 2002.

65. Amorosi, A.; Sammartino, I.; Sarti, G. Background levels of potentially toxic metals from soils of the Pisa coastal plain (Tuscany, Italy) as identified from sedimentological criteria. *Environ. Earth Sci.* **2013**, *69*, 1661–1671. [CrossRef]

66. Pal, S.K.; Roy, R. Evaluating heavy metals emission' pattern on road influenced by urban road layout. *Transp. Res. Interdiscip. Perspect.* **2021**, *10*, 100362. [CrossRef]

67. Zheng, S.-A.; Wu, Z.; Chen, C.; Liang, J.; Huang, H.; Zheng, X. Evaluation of leafy vegetables as bioindicators of gaseous mercury pollution in sewage-irrigated areas. *Environ. Sci. Pollut. Res.* **2018**, *25*, 413–421. [CrossRef] [PubMed]

68. Rinklebe, J.; During, A.; Overesch, M.; Du Laing, G.; Wennrich, R.; Stärk, H.-J.; Mothes, S. Dynamics of mercury fluxes and their controlling factors in large Hg-polluted floodplain areas. *Environ. Pollut.* **2010**, *158*, 308–318. [CrossRef]

69. Coufalík, P.; Komárek, J. The use of thermal desorption in the speciation analysis of mercury in soil, sediments and tailings. *J. Anal. Chem.* **2014**, *69*, 1123–1129. [CrossRef]

70. Kissinger, H.E. Reaction kinetics in differential thermal analysis. *Anal. Chem.* **1957**, *29*, 1702–1706. [CrossRef]

71. Lord, F.M.; Kittelberger, J.S. On the determination of activation energies in thermal desorption experiments. *Surf. Sci.* **1974**, *43*, 173–182. [CrossRef]

72. Kim, K.-H.; Yoon, H.-O.; Jung, M.-C.; Oh, J.-M.; Brown, R.J.C. A simple approach for measuring emission patterns of vapour phase mercury under temperature-controlled conditions from soil. *Sci. World J. Artic.* **2012**, *2012*, 940413. [CrossRef]

73. Roseborough, D.; Gothelid, M.; Aune, R.E.; Seetharaman, S. The surface behavior of mercury on iron systems. *Metall. Mater. Trans.* **2006**, *37*, 1049–1056. [CrossRef]

74. Siegel, S.M.; Siegel, B.Z. Temperature determinants of plant-soil-air mercury relationships. *Water Air Soil Pollut.* **1988**, *40*, 443–448. [CrossRef]

75. Yang, J.; Shi, N.; Yan, B.; Wang, T.; Pan, W.-P. Removal of elemental mercury by solid sorbents at different temperatures: Variation of the desorption activation energy through thermal desorption analysis. *Fuel* **2022**, *307*, 121889. [CrossRef]

76. Biester, H.; Gosar, M.; Müller, G. Mercury speciation in tailings of the Idrija mercury mine. *J. Geochem. Explor.* **1999**, *65*, 195–204. [CrossRef]

77. Do Valle, C.M.; Santana, G.P.; Augusti, R.; Filho, F.B.E.; Windmöller, C.C. Speciation and quantification of mercury in Oxisol, Ultisol, and Spodosol from Amazon (Manaus, Brazil). *Chemosphere* **2005**, *58*, 779–792. [CrossRef] [PubMed]

78. Hojdová, M.; Navrátil, T.; Rohovec, J. Distribution and speciation of mercury in mine waste dumps. *Bull. Environ. Contam. Toxicol.* **2008**, *80*, 237–241. [CrossRef]

79. Amirbahman, A.; Kent, D.B.; Curtis, G.P.; Marvin-DiPasquale, M.C. Kinetics of homogeneous and surface-catalyzed mercury(II) reduction by iron (II). *Environ. Sci. Technol.* **2013**, *47*, 7204–7213. [CrossRef]

80. Barnett, M.O.; Harris, L.A.; Turner, R.R.; Stevenson, R.J.; Henson, T.J.; Melton, R.C.; Hoffman, D.P. Formation of mercuric sulfide in soil. *Environ. Sci. Technol.* **1997**, *31*, 3037–3043. [CrossRef]

81. O'Connor, D.; Hou, D.; Ok, Y.S.; Mulder, J.; Duan, L.; Wu, Q.; Wang, S.; Tack, F.M.G.; Rinklebe, J. Mercury speciation, transformation, and transportation in soils, atmospheric flux, and implications for risk management: A critical review. *Environ. Int.* **2019**, *126*, 747–761. [CrossRef]

82. Kumari, S.; Jamwal, R.; Mishra, N.; Singh, D.M. Recent developments in environmental mercury bioremediation and its toxicity, e review. *Environ. Nanotechnol. Monit. Manag.* **2020**, *13*, 100283. [CrossRef]

83. Frohne, T.; Rinklebe, J.; Langer, U.; Du Laing, G.; Mothes, S.; Wennrich, R. Biogeochemical factors affecting mercury methylation rate in two contaminated floodplain soils. *Biogeosciences* **2012**, *9*, 493–507. [CrossRef]

84. Lin, C.J.; Gustin, M.S.; Singhasuk, P.; Eckley, C.; Miller, M. Empirical models for estimating mercury flux from soils. *Environ. Sci. Technol.* **2010**, *44*, 8522–8528. [CrossRef] [PubMed]

85. Grassi, S.; Netti, R. Sea water intrusion and mercury pollution of some coastal aquifers in the province of Grosseto (Southern Tuscany—Italy). *J. Hydrol.* **2000**, *237*, 198–211. [CrossRef]